## Computational Fluid Dynamics Simulations of Heat Transfer Between the Dense-Phase of a High-Temperature Fluidized Bed and an Immersed Surface

José M. Soria, Mariana T. Zambon, and Germán D. Mazza

Instituto Multidisciplinario de Investigación y Desarrollo de la Patagonia Norte (IDEPA, CONICET-UNCo), Universidad Nacional del Comahue, Buenos Aires 1400, 8300-Neuquén, Argentina

DOI 10.1002/aic.12579 Published online March 4, 2011 in Wiley Online Library (wileyonlinelibrary.com).

The transient process of heat transfer between a high-temperature emulsion packet and the wall of an immersed surface is simulated using computational fluid dynamics (CFD). From these simulations, the total heat transfer coefficient and its radiant contribution due to the emulsion (dense) phase are evaluated. The results are compared with experimental data (Ozkaynak et al., "An experimental investigation of radiant heat transfer in high temperature fluidized beds," in Fluidization IV, 1983:371–378) and with predicted values from the generalized heterogeneous model (GHM), (Mazza et al., "Evaluation of overall heat transfer rates between bubbling fluidized beds and immersed surfaces," Chem Eng Commun., 1997;162:125–149). The CFD simulations are in good agreement with both, experimental data and theoretical GHM predictions and provide a reliable way to quantify the studied heat transfer process. Also, the GHM is validated as a practical tool to this end. © 2011 American Institute of Chemical Engineers AIChE J, 58: 412–426, 2012

Keywords: CFD simulation, heat transfer, fluidized bed, emulsion, immersed surface

#### Introduction

Heat transfer between a bubbling fluidized bed and an immersed surface has been a subject of intense research to arrive at reliable models for predicting bed-to-wall heat transfer rate. Even if there are many mechanistic models and empirical expressions in the literature to evaluate the global heat transfer coefficient between the wall surface and the bed, most of them have a limited applicability range. The properties of solid particles as well as the structure of the bed and operating conditions have a strong influence on the response of the models and predictive expressions. The

Correspondence concerning this article should be addressed to G. D. Mazza at gmazza@uncoma.edu.ar.

© 2011 American Institute of Chemical Engineers

biphasic nature of the bed and the distribution of particles between dense phase and bubbles are complex topics to be taken into account for modeling purposes.

## Transient nature of the heat exchange at the wall surface

The classical concept of packet renewal introduced by Mickley and Fairbanks<sup>1</sup> can be used to account for the transient nature of the heat exchange in the dense phase of a fluidized bed. According to this approach, during the operation of a bubbling fluidized bed, the immersed surface contacts, alternatively, portions of dense phase (called "packets") and bubble phase. The temperature of the dense phase packets before contacting the surface wall corresponds to the average temperature of the bed. As soon as the packets contact the

immersed surface, transient heat transfer occurs. The packet as a whole absorbs/releases heat during a period of time called "contact time," tc. During this time, it is supposed that the particles do not move until they are swept away by the action of bubbles, returning them to the bulk of the bed where they take back the average temperature of the bed. Chen<sup>2</sup> states that visual observations in actively bubbling beds indicate that the particle emulsion actually remains fairly static, until disturbed by bubbles rising through the bed. On the subject, the author points out that "3 decades after Mickley and Fairbank's article, the basic concept of packet model-surface renewal was experimentally confirmed by researchers who were able to measure transient variations of particle concentration at heat transfer surfaces."3 It is Chen's opinion<sup>2</sup> that, from a phenomenological point of view, the best approach for fluidized bed heat transfer may well be the "packet model."1

Alternatively, several authors have reported that particles near the surface-wall do not remain static and that particle motion affects the thermal history of the solids and the resulting heat transfer rates. Experimental evidence about particle motion near the wall has been reported by Chen and Louge, Sidorenko et al., and Molerus et al., and also some effort has been dedicated to the formulation of models which consider particle motion near the wall.<sup>7,8</sup>

Molerus et al.<sup>6</sup> have studied the particle mobility in the near-to-wall zone of a bubbling fluidized bed. The authors observed the behavior of particles in this zone and measured axial and lateral particle migration velocities and concluded that lateral migration dominates the heat transfer process when the length of the immersed probe is small.

Recently, Chen and Louge<sup>8,4</sup> have reported an extensive study concerning theoretical (Part I) and experimental (Part II) analysis of the heat transfer enhancement in dense suspensions of agitated solids. In these works, the role of the thermal history and the influence of the solids mobility are discussed. On the side of modeling, the authors modeled agitated grains immersed in conductive fluids by coupling the fluid and solid phases through a volumetric source term. Particle agitation is considered by means of the "granular temperature," which allows quantifying the momentum transmitted through an effective viscosity. These authors<sup>8</sup> state that the flat thermal wall induces local ordering and also point out the possible creation of fluid velocity fluctuations by fast-moving particles. Such fluctuations affect the heat exchanging between solid and gas by raising the heat transfer coefficient around individual solids spheres. Particles agitated in a fluid with thermal temperature gradients are, in this context, subject to a complicated surface temperature spatial distribution and, mainly, time history.

It is recognized that possible fluctuations of particles, mainly rotational movements can expose different faces of the solid to heat flux and, as a consequence, the thermal history of the particle can affect its behavior with respect to heat transport. Closely connected to Biot number values, the thermal history could take a relevant role in the formulation of a model for wall-to-bed heat transfer evaluation.

On this basis, we do accept that the eventual particle motion and thermal history can exert some influence on the magnitude of the wall-to-emulsion heat transfer rate in bubbling fluidized beds. In this context, it could modify the hy-

AIChE Journal

pothesis concerning the static position of particles in the packet approach. However, the results obtained by means of both MHG and computational fluid dynamics (CFD) simulations presented in this article are really in very good agreement with experimental data. Also, as we have discussed in this section, the recent papers published by J. C. Chen, among other authors, emphatically supports the packet theory. Consequently, in this work we will adopt the packet theory and the sketch of fixed particles composing the packet during the contact time will be adopted in simulations.

Further work in this domain could include the effect of possible particle motion on heat transfer.

On the basis of recognizing the dense phase contribution to heat transfer, and that of the bubble phase, the total heat transfer coefficient between a fluidized bed and an immersed surface can be expressed as:

$$h = h_D(1 - f_B) + h_B f_B (1)$$

where  $f_{\rm B}$  is the volumetric bubble fraction, which is assumed as coincident with the fraction of time that the surface is in contact with the bubbles. 9,10

For bubbling fluidized beds operating at temperatures >800 K, thermal radiation contributes significantly to the overall heat transfer. In this case, the radiant heat transfer coefficient can be written as:

$$h_{rad} = h_{rad,D}(1 - f_B) + h_{rad,B}f_B \tag{2}$$

Since heat penetration regions are normally smaller than the size of bubbles and dense phase packets, each contribution in Eqs. 1 and 2 can be evaluated independently.

The dense phase contribution, represented by  $h_D$  (Eq. 1), is normally much larger than that from the bubble phase. Then, the attention will be focused in this article on the evaluation of the dense phase contribution to heat transfer. A simplified approach will be used to evaluate the bubble contribution,  $h_{\rm B}$  (Eq. 1).

#### Mechanistic model for wall-to-bed heat transfer rate evaluation: Brief description of the generalized heterogeneous model for the dense phase

Extensive studies concerning the formulation of basic models founded on the physical mechanisms involved in the wall-to-bed heat transfer process have been reported in the literature. However, only a relatively small percentage of such contributions deal with the operation at high temperatures and the evaluation of the radiant component of heat transfer rate. Recently, Wang et al. 11 have proposed a model although the validation of their results was not performed at extreme conditions. According to the discontinuous nature of the packets, Mazza<sup>12</sup> and Mazza et al. 13,14 formulated and validated the generalized heterogeneous model (GHM), which is used in this work. The detailed formulation for the GHM has been given by Mazza and Barreto.<sup>13</sup> Here, we present a brief description of the main characteristics of the GHM, including the approximation adopted for the evaluation of bubble-phase contribution.

The GHM stems from the description of the solid phase as an assembly of particle layers parallel to the immersed surface, following the idea proposed originally by Gabor.<sup>15</sup> The appropriateness of a layered structure for the solid phase instead of a pseudo-continuous approach has been discussed elsewhere.<sup>16</sup> However, it was also shown<sup>16,13</sup> that in practice it is only necessary to retain the first layer of particles (in contact with the immersed surface) whereas the rest of the dense phase packet can be either described as a layered structure or as a pseudo-continuous medium, since differences between predicted heat transfer rates are not significant. The pseudo-continuous approach for the rest of the dense phase packet is preferable as it allows a simpler mathematical treatment.

It is acknowledged in the GHM that the temperature of the gas surrounding the first particle layer is not the same as the particle temperature. Is has been checked by Mazza and Barreto<sup>17</sup> that this discrimination is not necessary for the rest of the packet, as a consequence of smaller heat fluxes allowing thermal equilibrium between gas and particles. From these observations, two zones are identified in the GHM: the zone adjacent to the transfer surface comprising the first layer of particles and interstitial gas, described in a thermally heterogeneous way, and the pseudo-homogeneous zone consisting of a semi-infinite medium. A qualitative picture of the temperature profiles in the two zones defined for the GHM is given in Figure 1.

The evaluation of the net radiant flux at the wall is made by means of a two-flux approach (radiant backward and forward fluxes are represented in Figure 1) and the MHG involves a set of thermal and fluid-dynamic parameters allowing evaluating the contribution of dense phase to the total heat transfer coefficient, and the corresponding radiant coefficient. The conservation equations in both, heterogeneous and pseudo-homogeneous zones of the GHM are formulated in the classical unsteady conditions and they are solved in order to obtain the global coefficient of heat transfer between the wall and the dense phase and its radiant contribution. Mathematical details and correlations for thermal parameters used in calculations are explained in previous contributions by the authors.  $^{14}$  The evaluation of time-parameters ( $t_{\rm c}$  and  $f_{\rm B}$ ) and other fluid-dynamics variables are discussed below in this article since the correlations used in CFD simulations are the same used for MHG calculations, to maintain coherency in the comparisons.

#### Evaluation of heat exchange with the bubble phase

Up to the authors' knowledge, there has been no experimental attempt to isolate the effect of heat (or mass) transfer from bubbles to immersed surfaces, although it is worthwhile to recall the analysis made by Chandran and Chen. <sup>18</sup> The authors evaluated  $h_{\rm B}$  from experimental values of the total coefficient h by subtracting the solid and gas contributions in the dense phase. For estimating the bubble-phase heat transfer coefficient  $h_{\rm B}$ , the gas convective contribution ( $h_{\rm c,B}$ ) resulting from the own void plus the so called through flow, and the radiant contribution ( $h_{\rm rad,B}$ ) from the exchange between the surface and the solid particle at the bubble boundary should be considered. The effect of both mechanisms can be simply added if the void is considered as being a perfect transparent medium,

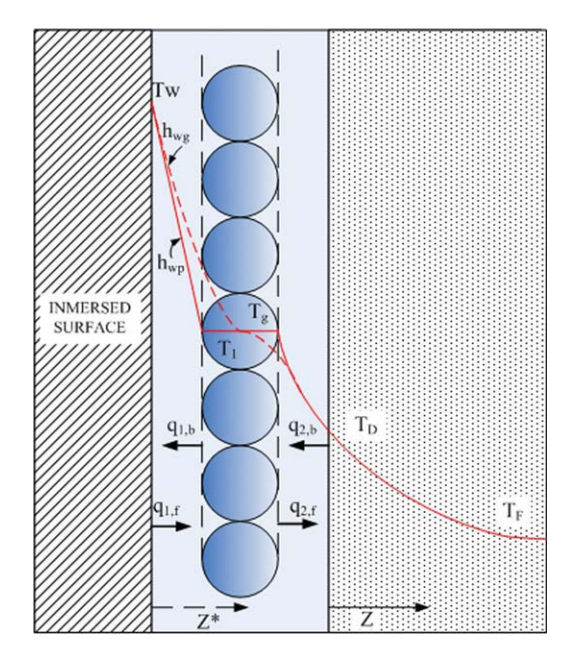


Figure 1. Sketch of the dense phase contacting an immersed surface according to the GHM.

[Color figure can be viewed in the online issue, which is available at wileyonlinelibrary.com.]

$$h_B = h_{c,B} + h_{rad,B}. (3)$$

An approximate expression to estimate the convective contribution has been proposed by Mazza and Barreto<sup>17</sup>:

$$h_{c,B} = 0.664 \left[ k_g \, c_{pg} \left( \frac{3 \, U_{mf} + u_B}{L_w} + \frac{3 \, U_{mf}}{L_B} \right) \right]^{0.5} Pr^{-0.17}$$
 (4)

where  $u_{\rm B}$  is the bubble rising velocity,  $d_{\rm B}$  is the bubble diameter, Pr is the Prandtl number, and  $L_{\rm B}=9d_{\rm B}/16$ . As regards the radiant heat exchange, based on the approach given by Yoshida et al.,<sup>19</sup> Mazza and Barreto<sup>20</sup> proposed the following approximated expression for  $h_{rad,B}$ 

$$h_{rad,B} = \sigma \left[ \frac{1}{\varepsilon_w} + F_{Bw} \left( \frac{1}{\varepsilon_D} - 1 \right) \right]^{-1} \left( T_w^2 + T_F^2 \right) (T_w + T_F) \quad (5)$$

and the emissivity of the internal bubble walls can be evaluated by the isothermal effective emissivity of the dense phase  $\varepsilon_{\rm D}$ . Equation 5 can be applied for the case of transparent wall, replacing the wall emissivity  $\varepsilon_{\rm w}$  by the emissivity of the second surface  $\varepsilon_{\rm S}$  and the corresponding temperature  $T_{\rm S}$  replaces the wall temperature. The exchange view factor  $F_{\rm Bw}$  can be estimated as  $F_{\rm Bw}=\min{(0.5,\gamma_{\rm A})}$  where  $\gamma_{\rm A}$  is proportional to the ratio between the area of the exchanging surface and that of the bubble, and depends on the geometry of the former (see Figure 2).

The main objective of this work is to simulate the transient process of heat transfer between high-temperature emulsion packet and an immersed surface by using CFD technique. Its results are compared with experimental data reported by Ozkaynak et al.<sup>21,22</sup> and also with predicted values from the application of the mechanistic GHM. As it was

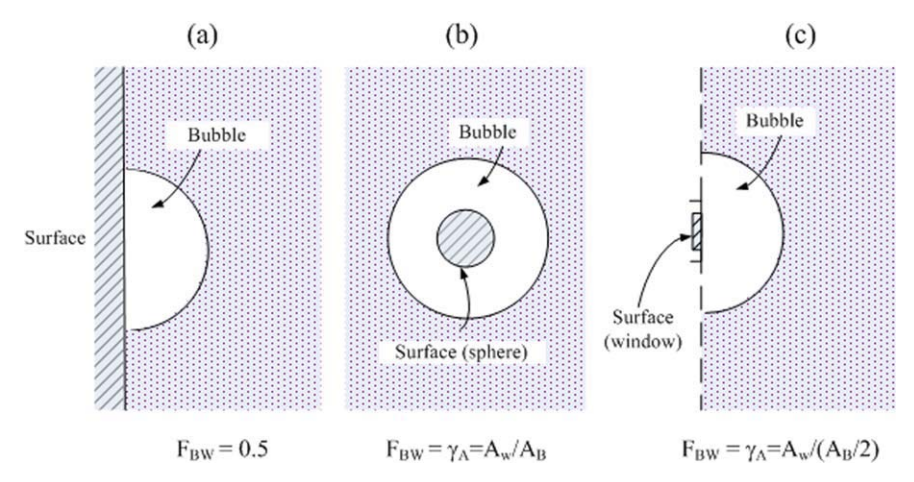


Figure 2. Configurations for analyzing radiant heat exchange between surface and bubbles.

mentioned above, the bubble phase contribution was estimated from approximated expressions (Eqs. 4-5) and it was subtracted from the experimental values of global heat transfer coefficient with the aim of obtaining the corresponding dense phase contribution (considered as an experimental value for comparison with simulations).

#### Heat transfer in gas fluidized beds: Previous experimental work

The experimental results reported in a relevant work in the field are considered here to compare bed-to-surface heat transfer coefficients with those calculated by CFD. These results correspond to bubbling regime of the bed and high operating temperature where radiative heat transfer is significant.

#### Ozkaynak et al.'s experiments<sup>21,22</sup>

These authors employed a radiometer probe, to measure the radiant and the total heat flux inside the experimental fluidized bed. The face of this probe was made of a cooper ring with a ZnSe transparent window at the center. The rest of the structure of the probe was constructed in brass.

It was found that the ZnSe window shows a high thermal conductivity and a wide transmittance band, which determines that it is more appropriate than frequently used quartz windows (which transmit only a small part of the radiation). A second window of the same material installed inside the probe received and transmitted only the radiant energy since the space between both windows was flushed with cooling air. The radiant flux was measured from the output of a thermopile, using an experimentally calibrated function. The whole probe was also cooled by water. The total amount of heat transferred from the bed was evaluated by the enthalpy change of the water and air flows. A distinguishing feature of this work is that the window temperature was measured and its uniformity was checked.

Two sizes of sand particles (average diameter 0.733 and 1.030 mm) were used and fluidized from 670 K up to 1031 K at superficial gas velocities reaching 5 m/s. The values of all physical properties of particles, probe dimensions, and operating conditions needed for simulating the heat transfer experiments, except  $U_{\rm mf}$  at operating temperature and  $\varepsilon_{\rm p}$ , were reported. A more detailed description of the hot-bed facility, calibration procedure for the probe, heat balance on the probe, collection of data, and the analysis of experimental data made by Ozkaynak et al., can be found in the original references. 21,22 The authors calculated the radiative heat transfer coefficients by:

$$h_{rad} = \frac{q_{rad}}{T_F - T_w} \tag{6}$$

and the total heat transfer coefficients were evaluated as:

$$h = \frac{q}{T_F - T_{wCu}} \tag{7}$$

where  $T_{\mathrm{wCu}}$  corresponds to the surface temperature of the

Bed and probe dimensions (bed diameter  $D_L$ , probe diameter  $d_{\rm T}$  and its distance from the distributor  $\varphi$ ) and also the values of particle thermo physical properties used to perform the CFD simulations are listed in Table 1.

#### CFD simulations: Methodology and time-parameter's evaluation

In this study, a rhombohedral array of spherical particles of uniform size is assumed to describe a dense phase packet

Table 1. Geometrical Characteristics and Particles Properties Used in This Study

Geometrical Characteristics	$D_{\rm L}$ (m)	$\varphi(m)$	$d_{\mathrm{T}}$ (m)	Particle	$d_{\rm p}~({\rm mm})$	$\rho$ (kg/m <sup>3</sup> )	k (W/m/K)	$C_{\rm p}~({\rm kJ/kg/K})$
Ozkaynak et al. <sup>21,22</sup>	0.45	0.381	0.073	Sand	1.030 0.733	2670	1.87	0.845

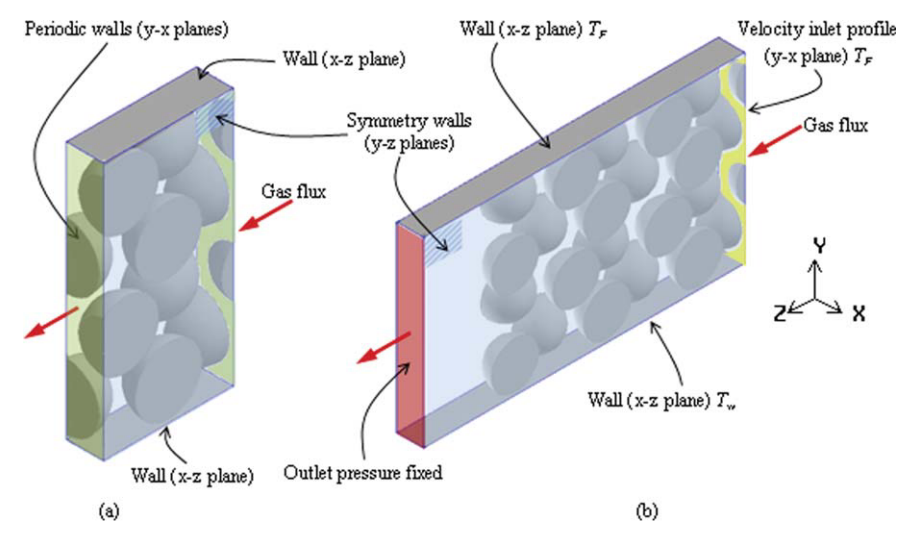


Figure 3. (a) Geometry used for obtaining velocity profile; (b) Geometry used in transient simulation.

at the wall. The array is envisaged to be developed from a compact layer of particles against the wall. The choice of a regular array largely facilitates the use of CFD, as will be discussed further below. On the other hand, the rhombohedral array has been shown to suitably approximate the behavior of the dense phase close to the wall surface. Moving away from the exchange surface, it is well known that the ordering effect produced by the surface starts to decay and the particles become more randomly distributed. However, since the thermal penetration depth does not grow up beyond one or at most two particle layers from the wall, for realistic values of the contact time  $t_c$ , there is no need to take into account explicitly the randomized inner zone of the packet.

The calculations to evaluate the heat transfer rate between the packet and the exchanging surface have been carried out in two stages. In the first one, a stationary velocity field in the zone close to the wall is evaluated. The width of the control volume (on the x coordinate, see Figure 3a) was taken as one particle's radius, taking advantage of symmetry. The length of the control volume (on the flow direction, see Figure 3a) spans along two staggered particles and was defined by two (x, y) planes (Figure 3a) placed in such a way that allows the setting of periodic boundary conditions. The depth of the control volume is defined by four layers of spheres bounded by the heat exchange surface and by an imaginary plane where bulk bed conditions were employed. This number of layers ensures that the velocity field is not longer affected by the non-slip condition at the heat exchange surface.

One distinguishing feature of this work is that the velocity profile at the entrance of the computational domain obtained from the first stage (plane z=0, Figure 3a) is then used as a boundary condition in the energy conservation equation, which is solved in the second stage to obtain, during the contact time  $t_c$ , the non-stationary velocity and temperature fields, and also the total and radiative average heat transfer rates.

The use of a velocity profile in this way avoids the needs of including a calm zone to achieve the condition of developed flow. On this basis, the influence of the hydrodynamic patterns on the heat transfer is rigorously considered.

The control volume is now of the same depth and width as before, but the length is extended up to six staggered particles (Figure 3b) to ensure that, for the conditions tested, the flow of gas does not modify the downstream temperature field. In turn, the depth of four particle layers was always safely longer that the heat penetration depth.

A mean void fraction in the dense phase of 0.5 was adopted, a typical value at minimum fluidization conditions. The rhombohedral array used in the calculations was expanded to achieve this value. In this way, particles neither touch each other nor touch the wall. The separation gap thus generated avoids the difficulties encountered for meshing the region around contact points, as was pointed out by Nijemeisland et al.<sup>23</sup>

Nonetheless, special care was taken in refining the mesh in the zones close to the separation gaps, as the gas flow contracts severely. Figures 4a, b show the mesh appearance within the gas-phase and solid phases. It was checked that the size of the final mesh was such to insure no significant change of the results reported in this contribution. As a result, the control volume used for the second stage of the procedure was divided into 1,568,344 cells.

The simulations were performed three-dimensionally using FLUENT 6.3.26 CFD code, on the basis of meshes built by using GAMBIT 2.4.6 software.

The fluidizing agent is air, which is considered as a non-participating medium for radiative mechanism. This means that it does neither absorb nor scatter the radiation. It is evaluated as a compressible fluid and its thermo-physical properties are evaluated as a function of temperature.

The immersed surface thermal boundary condition was established as the value of the window temperature reported by Ozkaynak et al.,  $T_{\rm w}$ .  $^{21,22}$ 

With respect to the initial temperature profile, the average bed temperature  $T_{\rm F}$  is assumed on the basis of the packet theory. This hypothesis allows considering that when the packet contacts the wall, its temperature is uniform and

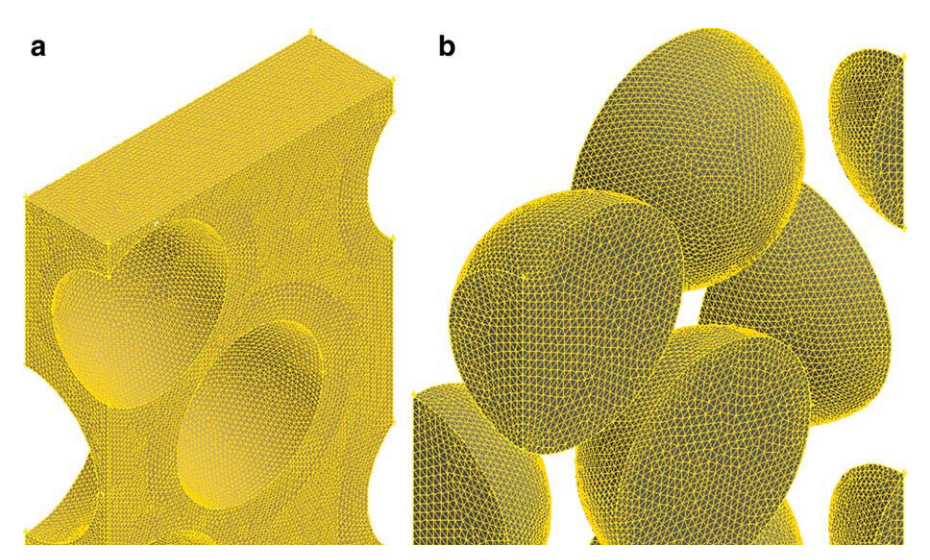


Figure 4. Mesh characteristics for (a) fluid and (b) solids.

equal to  $T_{\rm F}$ . This is a usual initial condition for modeling the gas contribution to heat transfer between an immersed surface and the dense phase of a fluidized bed. 1

As it has been remarked in previous section, the contact with the bubble phase (and the heat transfer involved) is not simulated by CFD at this stage of the work. The approximate approach described in the corresponding section was applied instead. Besides, gas convective mechanism in the bubble phase can be neglected in, and the particle convective contribution in bubbles is also usually negligible because of small particle concentration.<sup>20</sup>

#### Governing equations and radiative heat transfer

The software used solves numerically the usual Navier-Stokes equation, the local energy equation, and the radiation heat transfer equation in the fluid and solid phases.

The radiative transfer equation (RTE) for an absorbing, emitting, and scattering medium at position  $\vec{r}$  in the direction  $\vec{s}$  is

$$\frac{dI(\vec{r}, \vec{s})}{ds} + (\beta_{abs} + \beta_{sca})I(\vec{r}, \vec{s})$$

$$= \beta_{abs}n^2 \frac{\sigma T^4}{\pi} + \frac{\beta_{sca}}{4\pi} \int_0^{4\pi} I(\vec{r}, \vec{s}')\phi(\vec{s}, \vec{s}')d\Omega' \quad (8)$$

where  $\beta_{abs}$  is the absorption coefficient,  $\beta_{sca}$  the scattering coefficient, n the refractive index, and I the radiation intensity, which depends on position  $(\vec{r})$  and direction  $(\vec{s})$ . FLUENT provides different radiation models to solve Eq. 8, which allow including radiation in heat transfer simulations.

As it can be found in Fluent User's Manual, only the discrete ordinates radiation model (DOM) can be considered to be appropriate for the system dealt with in this paper. It is the only one allowing and simulating the behavior of semi-transparent walls (interior and exterior), which is necessary for analyzing the radiant effect inside solid surfaces. Also, opaque condition can be established for solid surfaces if necessary.

The DO radiation model solves Eq. 8 for a finite number of discrete solid angles, each associated with a vector direction  $\vec{s}$  in the global Cartesian system (x, y, z). The model transforms Eq. 8 into a transport equation for radiation intensity in the spatial coordinates (x, y, z). The DOM solves for as many transport equations as there are directions  $\vec{s}$ . The solution method is identical to that used for the fluid flow and energy equations.

Two implementations of the DOM are available in FLU-ENT: uncoupled and (energy) coupled. The uncoupled implementation is sequential in nature and uses a conservative variant of the DOM called the finite-volume scheme. In the uncoupled case, the equations for the energy and radiation intensities are solved one by one, assuming prevailing values for other variables.

Alternatively, in the coupled ordinates method (COMET), the discrete energy and intensity equations at each cell are solved simultaneously, assuming that spatial neighbors are known. The advantages of using the coupled approach are that it speeds up applications involving high optical thicknesses and/or high scattering coefficients. Such applications slow down convergence drastically when the sequential approach is used. The DOM with the COMET alternative was used in this work.

To perform simulations, some parameters and properties must be set in FLUENT environment. In the next two sections, a description of these requirements is included.

#### Parameters and fluid dynamics properties

The Reynolds number in the dense phase can be written as:

$$Re_D = \rho_g.U_D.d_p / \mu \tag{9}$$

where  $U_{\rm D}$  is the superficial gas velocity in the dense phase evaluated from the expression proposed by Decker and Glicksman.<sup>24</sup> Laminar regime was adopted for all simulations

Table 2. Expressions Used for Evaluating Fluid Dynamics
Parameters

$Re_{mf} = -57.09 + \left(1920 + 0.0564Ar^{1/1.07}\right)^{0.535}$ $d_B = 0.0123\left[1 + 27(U - U_{mf})\right]^{0.33}(1 + 6.84\varphi)^{0.5}$	Baeyens and Geldart <sup>25</sup> Hiligardt and Werther <sup>26</sup>
$t_c = 2.5 Z^{0.8} \left[ \frac{d_p}{U - U_{mf}} \right]^{0.5} \left[ \frac{(\rho_p - \rho_g)(1 - \delta_{mf})}{\rho_g} \right]^{0.4}$	Bock <sup>27</sup>
$f_B = 0.15Z^{-0.65} \left( \frac{U - U_{mf}}{\sqrt{g d_e}} \right)^{0.5}$	Book
In this work, $Z = \varphi$ and $D_L$	
$U_D = \mathrm{U}_{mf} \left( 1 + 2f_B \right)$	Decker and Glicksman <sup>24</sup>

because of the low  $Re_{\rm D}$  values. Consequently, the calculation time needed to complete the CFD simulation is shorter than that required in turbulent flows. Although fluidized beds have a remarkable thermal uniformity, an important thermal gradient in the zone near the exchange surface wall is developed, mainly for distances less than a particle diameter, where the influence of  $t_c$  is significant. Taking into account that  $h_D$  has a strong dependence on the fluid thermo physical properties: density, viscosity, calorific capacity, and thermal conductivity (besides the superficial gas velocity), temperature dependent fluid properties are used. The fluid dynamic parameters are calculated according to the correlations shown in Table 2. To achieve the correct comparison with CFD results, these correlations are the same ones used for calculating the heat transfer coefficients from the GHM. A discussion concerning main time-parameters ( $f_{\rm B}$ ,  $t_{\rm c}$ ) because of their major role in heat transfer rate evaluation is included in next section.

#### Time-parameters evaluation

As it has been remarked by Chen, a problem in using the surface-renewal approach is the lack of reliable information on the two time-parameters ( $t_c$  and  $f_B$ ). In this article, the empirical correlation of Bock<sup>27</sup> was applied for the evaluation of both  $t_c$  and  $f_B$  operating values. The correlation of Bock was selected because this author formulated its expressions on the basis of extensive measurements of the fluid dynamic properties in fluidized bed and they were tested over a wide range of operating conditions (i.e., bed diameter, materials and gases, temperature, pressure, and excess gas velocity) but, as one of the most important feature, the gas—solid system dealt with in our article (sand/air) was particularly analyzed by Bock. Experimental results reported by Bock were well fitted by the heat transfer model proposed by the author including its formulation for the time parameters described in this paragraph.

However, with the aim of verifying the behavior of Bock's expressions, we have compared the values of  $t_c$  and  $f_B$  provided by this correlation with an experimental set of results from the literature.

Chen<sup>2</sup> based on the measurements of Ozkaynak and Chen<sup>3,28</sup> reported empirical curves for the mean residence time and time fraction for the emulsion  $f_{\rm D}=(1-f_{\rm B})$  as functions of the excess gas velocity  $(U-U_{\rm mf})$ . The author observes that both the mean residence time  $(t_{\rm c})$  and time fraction for the dense phase  $f_{\rm D}$  decrease with increasing  $(U-U_{\rm mf})$  for particles of a given size, and increase with increasing particle diameter. For vigorously bubbling beds, the residence time of particle packets on a heat transfer sur-

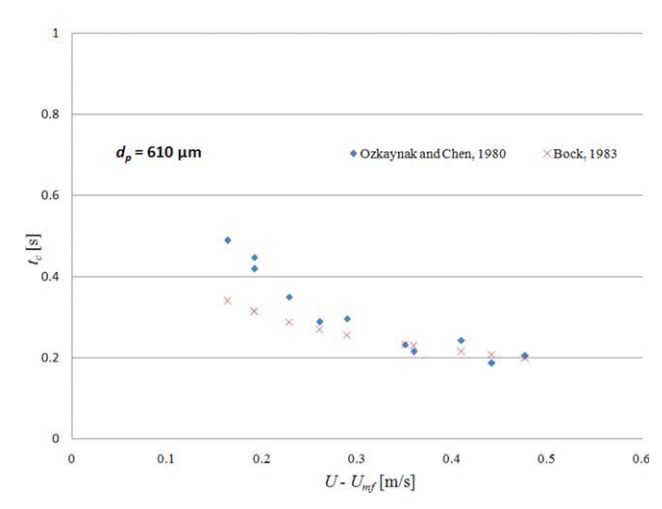


Figure 5. Comparison of experimental emulsion phase contact time  $t_{\rm c}$  at local position on heat transfer surface from Chen<sup>3,28</sup> with calculated values from Bock's expression.<sup>27</sup>

[Color figure can be viewed in the online issue, which is available at wileyonlinelibrary.com.]

face tends to be on the order of <1 s. Although the values of  $t_c$  calculated from Bock's correlation for our study are in good agreement with this observation, we have checked the behavior of this correlation with respect to the experimental values reported by Chen.<sup>2</sup>

Experimental values of  $t_{\rm c}$  and  $f_{\rm D}$  are plotted in Figures 5 and 6, respectively. They correspond to measurements carried out with spherical glass particles ( $d_{\rm p}=0.610$  mm) fluidized in ambient air.<sup>2</sup> Also, values from Bock's empirical expressions are included in the figures.

A good agreement between predicted and experimental values of  $f_D$  can be appreciated in Figure 6. The average of absolute relative errors is e% = 6%. A similar conclusion arises from contact time comparison plotted in Figure 5. In

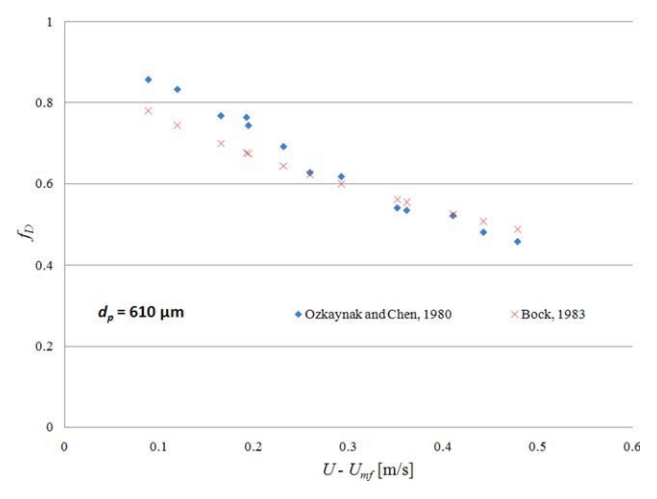


Figure 6. Comparison of experimental time fraction for packets  $f_D$  at local position on heat transfer surface from Chen<sup>3,28</sup> with calculated values from Bock's expression.<sup>27</sup>

[Color figure can be viewed in the online issue, which is available at wileyonlinelibrary.com.]

Table 3. Optical Properties Used in CFD Simulations

	Case of Ozkaynak et	al.'s Experiments <sup>21</sup>	,22
d <sub>p</sub> (mm)	m	$\beta_{\rm abs}~({\rm m}^{-1})$	$\beta_{\rm sca}~({\rm m}^{-1})$
0.733	1.3 - 0.001i	1673.34	2487.55
1.030	1.3 - 0.001i	1290.83	1655.44

this case, e%=10.5%. The agreement is excellent for the higher values of  $(U-U_{\rm mf})$ .

From the observations described above, considering that the experimental high-temperature heat transfer rate values were also reported by Ozkaynak and Chen, and that the Bock's expressions reproduces well the values of the two key time parameters, we conclude that this correlation can be used for the objective of our article.

It is interesting to note here that Bock's correlation also reproduces well the order of magnitude of experimental values of contact time reported by Hamidipour et al.<sup>29</sup>

A sensitivity analysis of the behavior of simulations on these parameters is also included later in this article.

#### Optical properties

As it has been described above, the software requires optical properties values to solve the radiative heat transfer equation in the frame of discrete ordinates method. These properties are  $\beta_{\rm abs}$ ,  $\beta_{\rm sca}$ , and n. For the estimation of absorbing ( $\beta_{\rm abs}$ ) and scattering ( $\beta_{\rm sca}$ ) coefficients, Mie theory is applied. Calculations from this theory require in turn the complex refractive index  $m=n-k_{\rm a}$  i, where  $k_{\rm a}$  is the absorption index, the value of the wavelength at mean bed operating temperature and the particle diameter  $d_{\rm p}$ .

Hua et al.<sup>30</sup> have reported that 80% fraction of radiation power is in the wavelength range  $0.5-7~\mu m$  at about 1100 K for fluidized bed combustors. Therefore, most attention is paid to the optical constants for  $\lambda < 7~\mu m$ . Lacroix et al.<sup>31</sup> measured the n and  $k_a$  values for sand particles using the Kramers-Kronig transform of the signals, indicating that the material is not gray and the optical constants (n and  $k_a$ ) have a strong dependence on the wavelength. However, the authors also reported that  $\beta_{abs}$  measured for temperatures in the range of 1073–1473 K show a slight variation for wavelengths between 1  $\mu m$  and 4.5  $\mu m$ .

Only a few contributions deal with optical properties of silica sand particles. Yamada et al.<sup>32</sup> reported that n is about 1.3 and the absorption index is about  $10^{-3}$ . These values were used in simulations.

On the basis of the observations of Lacroix et al.,<sup>31</sup> the  $\beta_{abs}$  were calculated in a first approximation as well as  $\beta_{sca}$  values by means of a code for Mie theory calculations, and then all the simulations are performed with constant values of the absorption and scattering coefficients.

**Table 4. Main Solving Parameters** 

Variable	Under-Relaxation Factor	Discretization
Pressure	0.5	PRESTO
Momentum	0.5	Second order upwind
Energy	0.95	Second order upwind
Discrete Ordinates	0.95	Second order upwind

Table 5. Discretization Scheme Comparison

	$d_{p}$	Discre	Order tization neme	Discre	d Order tization neme	Relative Error for	Relative Error for
	(mm)	$h_{\mathrm{rad,D}}$	$h_{\mathrm{D}}$	$h_{\rm rad,D}$	$h_{ m D}$	$h_{\mathrm{rad,D}}$ (%)	$h_{\rm D}~(\%)$
Ī	0.733 1.030	32.78 69.09	321.44 318.40	32.76 69.06	321.74 318.65	0.061 0.048	-0.093 $-0.077$

Finally, from Hua et al.'s reported results, a value of wavelength of 4  $\mu$ m is adopted in simulations. Table 3 shows the values of complex refractive indexes and the resulting absorption and scattering coefficients for the experiments used in simulations. A value of  $\varepsilon_p = 0.71$  is taken for the sand particles from Liley<sup>33</sup> in CFD and GHM calculations.

#### Numerical solution

The pressure-based method is applied to solve the Navier-Stokes equation due to the low gas velocity. The appropriate under-relaxation factors are set to avoid instability in the solution, reaching convergence in lower number of iterations. Table 4 resumes the main numerical solving parameters used in the simulations. They correspond to a second order discretization scheme for momentum and energy variables. Several simulations were run to validate the selected numerical scheme. In particular, the referred second order scheme was compared to a more accurate option (a third order MUSCL scheme). The Nusselt number or the corresponding heat transfer coefficients were adopted as criteria for evaluating the performance of the numerical scheme. In this sense, Table 5 resumes the numerical results obtained for two particle sizes  $d_{\rm p}=0.733$  mm and  $d_{\rm p}=1.030$  mm and bed temperature values  $T_{\rm F} = 799.2$  K and  $T_{\rm F} = 1010.5$  K, respectively. Very low errors are obtained when the second order discretization scheme for the evaluation of both radiant and total heat transfer coefficients is applied. Even more, computing times for the second order discretization scheme are slightly shorter. Additional information is presented in Figure 7 where y velocity component values, evaluated from both second and third order discretization scheme, are plotted as a

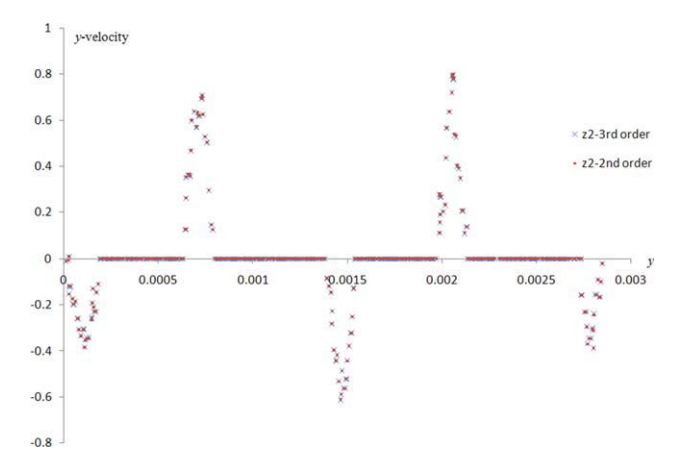


Figure 7. Comparison between numerical schemes based on y velocity component values.

[Color figure can be viewed in the online issue, which is available at wileyonlinelibrary.com.]

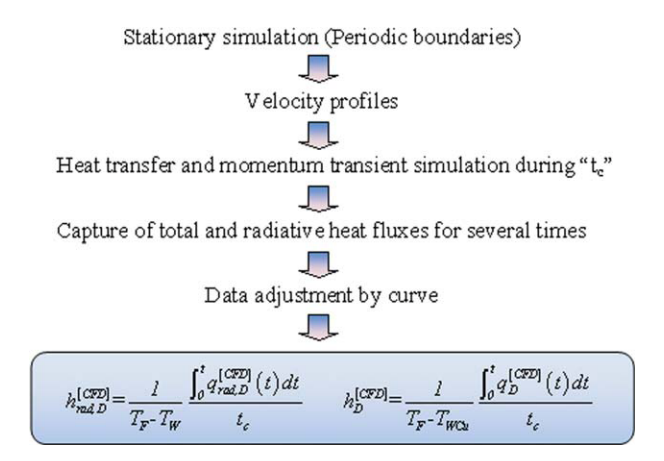


Figure 8. Scheme representing the post-treatment procedure.

function of y coordinate, where the zero values of velocity correspond to spheres positions in the geometry. As it can be observed in the figure, the values are practically coincident (the relative average error is 0.57%). These observations provide evidence enough to support the selection of a second order discretization scheme. In this context, the second order discretization scheme was finally adopted for simulations.

The radiative heat transfer equation is solved using the DOM. The particles are considered as opaque bodies (although semitransparent conditions can also be adopted if necessary). The pixilation and angular discretization required by DOM in the frame of FLUENT are established at  $3\times 3$  and  $2\times 2$ , respectively. An increase of these parameters does not produce significant differences in the results (<1.5%) but a substantial enhance of computational time.

As it was pointed out in the CFD Methodology section, the thermal boundary condition of the heat exchange surface is established by setting the wall temperature  $T_{\rm w}$  with no absorption and scattering. For the gas entering the control volume, a velocity profile is used as a velocity inlet boundary condition; meanwhile the pressure is set at the end of the geometry. The fluid temperature at the geometry entrance is fixed according to the values reported by the authors as bed temperature  $T_{\rm F}$ . Finally, the opposite wall to the heat transfer surface is considered to be representative of the packet, with  $T_{\rm F}$  and emissivity calculated from the expres-

sion proposed by Mazza and Barreto<sup>20</sup> for the isothermal emissivity of the dense phase. Like the exchange surface, this wall is specified as a stationary wall with no slip.

The simulations are carried out in transient state, with a step size of 0.01 s. In both cases, the number of iteration per step is set to 50 and all the residuals to  $10^{-9}$ . In each time step, the radiant and total heat fluxes on the exchange surface are calculated. Those values are fit, obtaining as a result an equation for each flux as a function of time. Then, the heat transfer coefficients can be obtained. The sequence describing the post-treatment procedure for obtaining the total and radiant heat transfer coefficients can be appreciated in Figure 8.

#### **Results and Discussion**

Tables 6 and 7 resume the values of  $h_{\rm rad,D}$  and  $h_{\rm D}$  for several of the experiences reported by Ozkaynak et al.,<sup>21,22</sup> the calculated values from GHM and those obtained by the CFD for the smaller and bigger particles, respectively.

A very good agreement is achieved between the values of  $h_{\rm rad,D}$  and  $h_{\rm D}$  calculated by the GHM and the experimental results and also between the last ones and the results of the CFD simulations. CFD calculations allow gathering new evidence of the GHM applicability.

Figures 9 and 10 show the values of the radiative and total heat transfer coefficients due to emulsion phase, respectively. Results listed in Tables 6 and 7, for  $d_p = 0.733$  mm and  $d_p$ = 1.030 mm, are also included in the figures. As expected, the  $h_D$  values for the smaller particle diameter are always higher than those for larger particles. Differences between CFD values and experimental data are not too significant. Among the possible factors causing these differences, the optical properties and operating parameters estimation can be mentioned. The optical properties of the particles play a very important role on  $h_{\rm rad,D}$  and particularly in calculations when CFD is used. There is a great uncertainty in the absorption index of sand. According to Yamada et al.,32 the value of this index can vary from  $10^{-2}$  to  $10^{-4}$ . Moreover, these authors show how a decrease in the value of  $k_a$  increases  $h_{\rm rad,D}$ . This takes place because when  $k_{\rm a}$  diminishes an increase in the radiation penetration depth occurs. Possible particle motion and corresponding thermal-history can also produce differences with respect to experimental data, as it has been discussed in the Introduction. Finally, as regard the

Table 6.  $h_{\text{rad,D}}$  y  $h_{\text{D}}$  Values for CFD, MHG, and Ozkaynak et al.<sup>21,22</sup> ( $d_{\text{p}} = 0.733$  mm)

		Ozka	ıynak et a	ıl. <sup>21,22</sup>			_	M	HG			CI	FD (this v	vork)		
Exp. No.	$T_{\rm F}$ (K)	$T_{\rm w}$ (K)	$T_{\text{wCu}}$ (K)	U (m/s)	$h_{\rm rad,D}$	$h_{ m D}$	$h_{\rm rad,D}$	e%	$h_{ m D}$	e%	$q_{\rm rad,D} \over ({ m W/m}^2)$	$q_{\rm D}$ $({ m W/m}^2)$	$h_{\rm rad,D}$	e%	$h_{ m D}$	e%
1	1016.4	471.7	412.35	3.313	67.34	450.59	74.19	-10.2	411.32	8.7	35052.7	261030.5	70.25	-4.3	404.56	10.2
2	967.4	457.2	397.25	1.952	67.09	386.37	58.82	12.3	422.56	-9.4	30174.2	204558.4	59.142	11.8	358.78	7.1
3	799.2	366.9	354.5	1.442	39.9	328.71	32.57	18.4	360.13	-9.6	20541.6	168296.2	32.76	17.9	321.74	2.1
4	1031.3	488.1	423.05	1.520	79.38	417.42	63.32	20.2	454.25	-8.8	12291.5	137239.8	64.53	18.7	429.15	-2.8
5	873.8	436	389.55	2.25	53.57	407.38	48.49	9.5	381.04	6.5	14162.1	143079.6	46.92	12.4	347.54	14.7
6	769.7	336.9	350.45	1.386	34.14	337.17	28.13	17.6	344.71	-2.2	36820.3	241584.4	28.4	16.8	327.35	3
7	1016.3	413.4	390.45	1.948	58.68	411.81	60.57	-3.2	423.66	-2.9	38265.2	244374.5	61.07	-4.1	386.01	6.3
8	962.1	449.9	389.65	1.975	67.42	391.97	57.80	14.3	418.21	-6.7	29629.2	204215.8	57.84	14.2	356.74	8.9
9	1010.6	409.3	390.4	1.815	59.07	375.85	58.19	1.5	423.09	-12.6	35791.8	237238.9	59.52	-0.8	382.52	-1.8
10	1005.7	415.7	397.35	1.806	56.66	416.75	58.11	-2.6	423.66	-1.7	35120.3	232876.4	59.52	-5.0	382.8	8.2

Table 7.  $h_{\rm rad, D}$  y  $h_{\rm D}$  Values for CFD, MHG, and Ozkaynak et al.<sup>21,22</sup> ( $d_{\rm p}=1.030~{\rm mm}$ )

											-					
			Ozkaynak et al	et al. <sup>21,22</sup>				M	MHG				CFD (This Work	/ork)		
Exp. No.	$T_{ m F}$ (K)	$T_{\rm w}$ (K)	$T_{ m wCu} \  m (K)$	U (m/s)	$h_{\rm rad,D}$ (W/m <sup>2</sup> /K)	$h_{\mathrm{D}}$ (W/m <sup>2</sup> /K)	$h_{\rm rad,D}$ (W/m <sup>2</sup> /K)	e%	$h_{\mathrm{D}}$ (W/m <sup>2</sup> /K)	6%	$q_{\rm rad,D}$ $({ m W/m}^2)$	$q_{\rm D}$ $({ m W/m}^2)$	$h_{\mathrm{rad,D}}$ (W/m <sup>2</sup> /K)	6%	$h_{\mathrm{D}}$ (W/m <sup>2</sup> /K)	6%
1	863.3	400.9	368.65	3.166	52.04	270.62	46.60	10.5	302.62	-11.8	21230.1	145860.4	45.91	11.8	294.88	-9.0
2	957.7	420.9	382.05	3.714	60.36	317.30	61.31	-1.6	325.63	-2.6	32542.1	175821.7	60.622	-0.4	305.43	3.7
3	959.7	423	381.55	3.6	60.58	302.07	61.24	-1.1	330.76	-9.5	32464.5	185580	60.49	0.1	320.99	-6.3
4	981.6	430.9	387.65	3.779	64.27	323.58	65.62	-2.1	335.66	-3.7	35532.6	195491.5	64.52	-0.4	329.14	-1.7
5	867.3	408.7	372.35	3.259	49.30	293.89	47.94	2.8	303.06	-3.1	21647.1	146525.1	47.26	4.1	296.04	-0.7
9	787.2	396.2	365.25	2.899	38.62	311.00	37.68	2.4	283.51	8.8	14502.5	115641	37.09	4.0	274.06	11.9
7	1022	448.1	394.15	2.909	71.21	318.33	64.64	9.2	350.21	-10	40747.4	200525.9	71	0.3	319.384	-0.3
8	891.4	409.1	373.95	3.346	51.87	276.84	50.98	1.7	309.26	-11.7	24228	157121.7	50.234	3.2	303.65	7.6-
6	937.5	415.8	379.95	4.113	57.35	327.70	60.22	-5.0	303.77	7.3	29970.7	183150.9	57.448	-0.2	328.48	-0.2
10	1010.5	445.3	396.9	2.867	71.28	298.69	62.86	11.8	330.09	-10.5	39034.5	195522.6	90.69	3.1	318.65	<b>-6.7</b>
																Ī

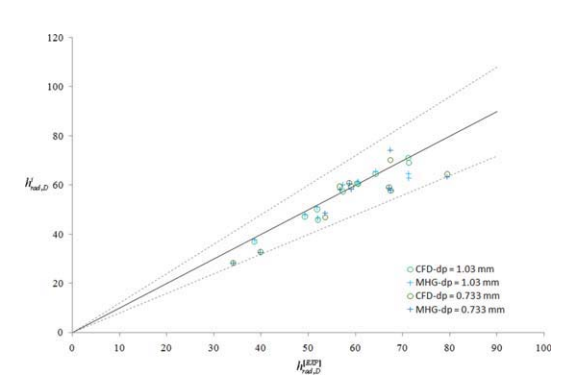


Figure 9.  $h_{\rm rad,D}$  comparison between experimental values, CFD, and GHM calculations.

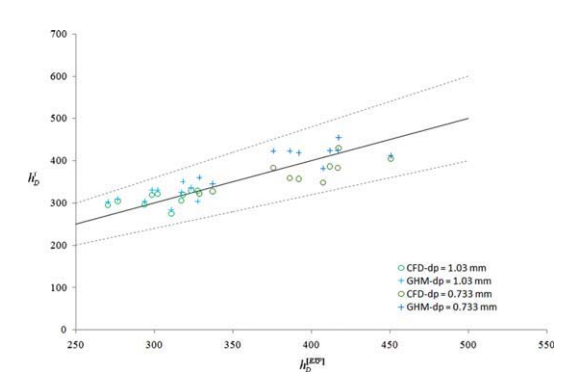


Figure 10. h<sub>D</sub> comparison between experimental values, CFD, and GHM calculations.

[Color figure can be viewed in the online issue, which is available at wileyonlinelibrary.com.]

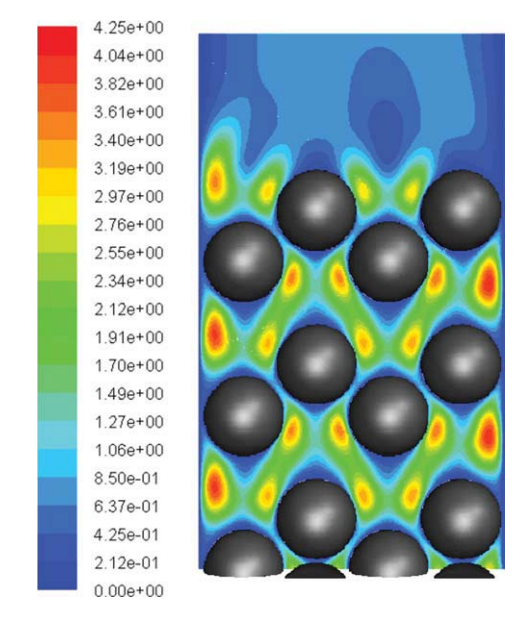


Figure 11. Velocity profile for experience 10,  $d_p = 1.030$  mm sand particles, U = 4.113 m/s at  $t = t_c$ .

[Color figure can be viewed in the online issue, which is available at wileyonlinelibrary.com.]

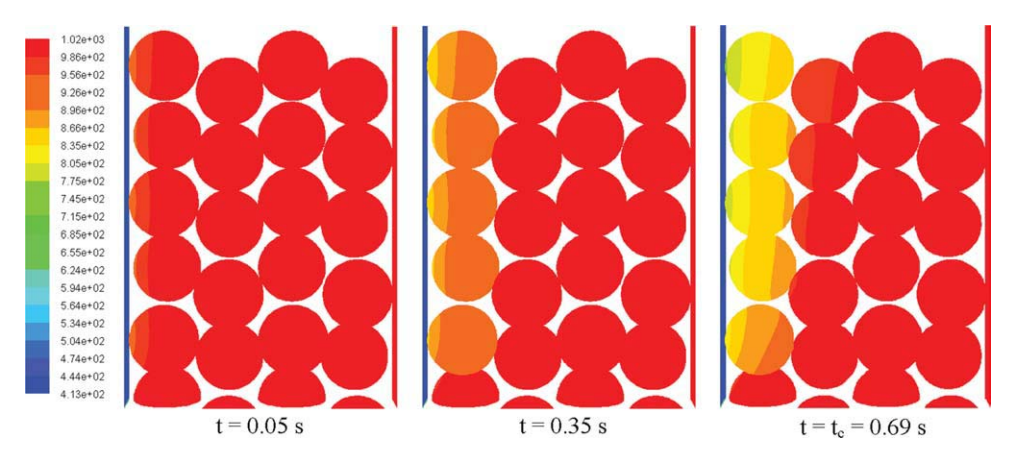


Figure 12. Thermal perturbation evolution for  $d_p = 0.733$  mm sand particles (CFD results).

Experience 7,  $T_{\rm F}=1016.3$  K,  $T_{\rm w}=413.4$  K, U=1.948 m/s,  $t_{\rm c}=0.69$  s. [Color figure can be viewed in the online issue, which is available at wileyonlinelibrary.com.].

parameters estimation, it is referred to later in the sensitivity analysis section.

The CFD software allows obtaining varied results which are interesting for describing the transient transport processes taking place between the emulsion packet and the surface wall. It concerns both the fluid dynamics and thermal behavior. In this sense, the velocity field obtained by CFD simulation at the final contact time for a typical experience is reproduced in Figure 11. The fluid dynamic pattern corresponding to a laminar flow regime can be visualized in the figure. With respect to the thermal behavior of the packet, Figures 12 and 13 show the temperature profiles in the nearwall zone for a temporal sequence including the final contact time value. This sequence is presented for two experiences corresponding to both particle diameters.

It can be observed that for particles with  $d_p = 0.733$  mm (Figure 12), the thermal perturbation clearly advances towards the center of the packet as a function of time up to achieving the corresponding  $t_c$  value. In this case, the heat penetration depth practically reaches the particle diameter. However, the thermal perturbation does not always produce a significant heat penetration depth. In general, the smaller the particles the deeper the thermal perturbation can advance. So, for particles of  $d_p = 1.030$  mm, this effect is almost not produced (for operating conditions leading to the temperature fields showed in Figure 13). Only for the final value of time (close to the removal of the packet by the action of a bubble) a week change in color indicates some small change in particle temperature for the first layer of solids. The particles, in this case, remain at a thermal level close to  $T_{\rm F}$  during the whole contact time period. It can also be explained in terms of the Biot number,  $Bi = h_{pg}(d_p/2)/k_s$ . For Bi << 1, a uniform temperature profile can be expected inside the particles. In the present case, Biot number takes values close to 0.2, which are not small (eventual particle motion could improve the agreement with experimental heat transfer coefficients data if considered).

From the analysis of the mechanisms acting in the heat transfer process, the difference observed in the behavior of different size particles can be explained as follows.

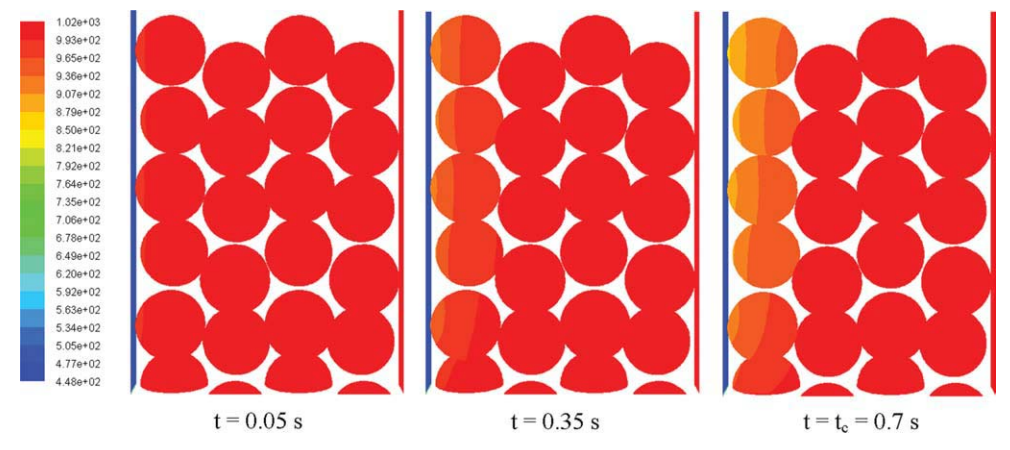


Figure 13. Thermal perturbation evolution for  $d_{\rm p}=1.030$  mm sand particles (CFD results).

Experience 8,  $T_F = 1022$  K,  $T_w = 448.1$  K, U = 2.909 m/s,  $t_c = 0.7$  s. [Color figure can be viewed in the online issue, which is available at wileyonlinelibrary.com.].

Table 8. Influence of Dense Phase Porosity on Heat Transfer Coefficients ( $d_p = 1.030$  mm; Experience 9)

Dense Phase Voidage		at Transfer ficient	Radiant C	Contribution
$\delta_{ m D}$	h	e%	$h_{\rm rad}$	е%
0.4	250.85	-2.810	66.515	0.5
0.45	246.91	-1.193	66.784	0.0987
0.5	244.48	-0.198	66.91	-0.089

The heat transfer rate from the dense phase to an immersed surface wall is determined by the action of three mechanisms: transient conduction in solid particles (caused by particles motion), interstitial gas convection and radiation. These mechanisms are obviously coupled but it is possible to find operating conditions where some of them could be dominant. The relative importance of gas convection and particle conduction is primarily defined by particles size. The gas convective contribution increases with particle diameter (higher velocities are required to fluidize larger particles) meanwhile the conductive contribution diminishes with  $d_{\rm p}$ , as the lenticular shaped gas regions between the wall and the first row of particles become thicker. In this case, the thermal perturbation is confined to a very narrow gas zone close to the wall but particles remain practically at

bulk bed temperature  $T_{\rm F}$ . For small particles, for example,  $d_{\rm p}$  < 0.5 mm, solid conductive contribution becomes significant (depending also on operating temperature and pressure).

Finally, as the application of CFD to this problem has required the selection of values for many parameters, a sensitivity study for the most relevant ones is included below, to show the importance of finding appropriate predictive expressions or experimental data for its evaluation.

### Sensitivity analysis on relevant parameters in CFD simulations

A sensitivity study was carried out with the aim of establishing the influence of a set of relevant parameters on the heat transfer rates obtained in CFD simulations. From the values obtained in the frame of the numerical scheme described above, the parameters were varied over reasonable ranges.

The study was performed for analyzing the influence of the dense phase voidage, the contact time, the dense phase time fraction  $f_D$ , or the equivalent  $(1 - f_B)$ , and absorption and scattering coefficients.

# Influence of the dense phase voidage on the dense phase total heat transfer coefficient and radiant contribution

With exception of small particles (Geldart's type A particles), values of dense phase voidage  $\delta_D$  are similar to  $\delta_{mf}$ .

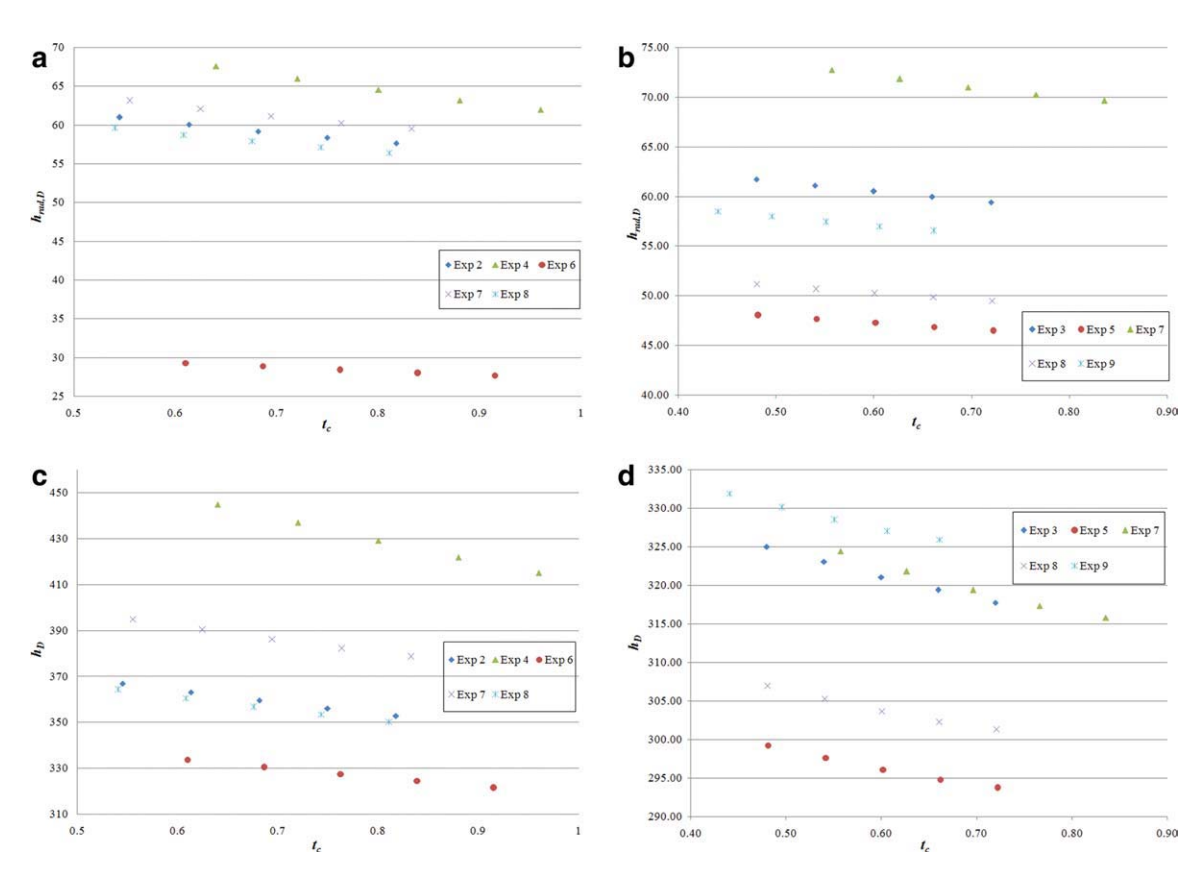


Figure 14. Influence of dense phase contact time on  $h_{rad,D}$  values: (a)  $d_p = 0.733$  m and (b)  $d_p = 1.030$  m. Influence of dense phase contact time on  $h_D$  values: (c)  $d_p = 0.733$  m and (d)  $d_p = 1.030$  m.

[Color figure can be viewed in the online issue, which is available at wileyonlinelibrary.com.].

As established earlier, a value  $\delta_{\rm D}=0.5$  was used in this work in both, MHG and CFD calculations.

It has been reported by Mazza and Barreto20 on the basis of MHG predictions, that the value of the emulsion porosity has little effect on the evaluation of total and radiant heat transfer coefficients. It was checked by the authors that a variation from  $\delta_{\rm D}=0.4$  to  $\delta_{\rm D}=0.5$  causes differences of about 2%.

With respect to CFD simulations, Table 8 resumes the influence of varying the  $\delta_{\rm D}$  in the range of 0.4–0.5. As it can be appreciated, the emulsion voidage seems not to present a significant effect on both, radiant and total heat transfer coefficients (differences of about 3% were found for the total coefficients whereas <1% can be observed for the radiant contribution).

#### Influence of packet contact time

Starting from  $t_c$  values calculated from Bock's correlation, a variation of 20% in both positive and negative sense (to consider eventual deviations of Bock's correlation from real contact time values) allows obtaining the results given in Figures 14a-d. It can be appreciated from the figures, that both  $h_{\text{rad},D}$  and  $h_{\text{D}}$  decrease when contact time increases, as expected. This can be explained by the drop of temperature of particles touching the surface that causes the thermal driving force to decline, resulting in a lower heat transfer coefficient. This analysis reveals the importance of a good evaluation of the contact time, which can be defined as the most important parameter for the heat transfer process studied here.

#### Influence of time fraction of bubble phase $(f_B)$ or, in terms of emulsion phase $(1 - f_D)$

The influence of  $(f_B)$  or, equivalently  $(I - f_D)$  on heat transfer coefficients values can be deduced from results given in Table 9. A perturbation of 20% in both, positive and negative sense, starting from Bock's predictions for a reference operating condition shows that this parameter is also one of the most relevant magnitude to evaluate (as observed in the previous analysis for  $t_c$ ).

#### Influence of absorption and scattering coefficients

The results concerning the influence of optical properties on heat transfer coefficients are presented hereafter. It is recognized<sup>30</sup> that the absorption index has more influence on the heat transfer coefficient than the refractive index. A sensitivity analysis is performed starting  $k_a$  (absorption index) from  $10^{-3}$ . Then, this value was modified to  $10^{-2}$  and  $10^{-4}$ . The corresponding absorption and scattering coefficients, along with the values of  $h_{\text{rad},D}$  and  $h_{\text{D}}$  are shown in Table 10. With respect to heat transfer coefficients obtained for each modified condition, it is observed in the table that  $h_{\rm rad,D}$  and  $h_{\rm D}$  increase strongly with  $k_{\rm a}$  between the range  $10^{-4}$ – $10^{-3}$ , and then it remains almost constant until the value of  $10^{-2}$ .

On the basis of the evidence exposed here, it is necessary to remark that the existent uncertainty of the value of this optical property determines the radiant heat transfer and, therefore, the total heat transfer coefficient.

						Tab	le 9. Influ	Table 9. Influence of fB in Heat Transfer Coefficients	B in Hear	t Transfe	r Coeffici	ents						
	I	Experience 4	+	H	Experience 2		E	Experience 5		E	Experience 6		E	Experience 3		Ex	Experience 7	
$d_{ m p}$	$f_{ m B}$	h	$h_{\rm rad}$	$f_{ m B}$	h	$h_{\mathrm{rad}}$	$f_{ m B}$	h	$h_{\mathrm{rad}}$	$f_{ m B}$	h	$h_{\rm rad}$	$f_{ m B}$	h	$h_{\rm rad}$	$f_{ m B}$	h	$h_{\rm rad}$
0.733	0.2704	349.39	78.40	0.3097	282.87	70.39	0.3336	262.64	55.88	0.2532	260.75	32.44	0.2595	256.81	37.70	0.3099	302.66	72.69
	0.2479	356.03	77.24	0.2839	289.20	69.45	0.3058	269.72	55.13	0.2321	266.30	32.10	0.2379	262.22	37.29	0.2840	309.61	71.72
	0.2254	362.68	76.09	0.2581	295.52	68.52	0.2780	276.79	54.39	0.2110	271.85	31.76	0.2163	267.64	36.88	0.2582	316.55	70.75
	0.2028	369.33	74.93	0.2323	301.85	67.58	0.2502	283.87	53.64	0.1899	277.40	31.43	0.1946	273.05	36.46	0.2324	323.50	82.69
	0.1803	375.97	73.77	0.2065	308.17	66.64	0.2224	290.94	52.89	0.1688	282.95	31.09	0.1730	278.46	36.05	0.2066	330.44	68.82
	I	Experience 1	1	E	Experience 5		E	Experience 6		E	Experience 7		E	Experience 8		Ex	Experience 9	
$d_{ m p}$	$f_{ m B}$	h	$h_{\mathrm{rad}}$	$f_{ m B}$	h	$h_{\mathrm{rad}}$	$f_{ m B}$	h	$h_{\mathrm{rad}}$	$f_{ m B}$	h	$h_{ m rad}$	$f_{ m B}$	h	$h_{\rm rad}$	$f_{ m B}$	h	$h_{\mathrm{rad}}$
1.030	0.3907	214.94	54.00	0.3971	215.04	55.68	0.3706	201.59	43.39	0.3748	247.67	84.17	0.4032	219.95	59.32	0.4520	227.68	68.80
	0.3581	221.60	53.33	0.3640	221.79	54.98	0.3397	207.63	42.87	0.3436	253.65	83.07	0.3696	226.92	58.56	0.4143	236.08	98.79
	0.3256	228.26	52.65	0.3309	228.54	54.28	0.3088	213.66	42.34	0.3124	259.62	81.98	0.3360	233.90	57.80	0.3766	244.48	66.91
	0.2930	234.92	51.98	0.2978	235.29	53.57	0.2779	219.70	41.82	0.2811	265.60	80.88	0.3024	240.87	57.05	0.3390	252.88	96:59
	0.2344	246.91	50.77	0.2382	247.44	52.31	0.2223	230.58	40.87	0.2249	276.36	78.90	0.2419	253.43	55.68	0.2712	268.00	64.26
Wolnes in	third row or	ot buonsens	Book's no	adiotions for	Walnes in third row correspond to Book's medictions for both A values	3011												

Table 10. Influence of Absorption and Scattering Coefficients in the Heat Transfer Coefficients

n	$k_{\rm a}$	$\beta_{ m abs}$	$\beta_{ m sca}$	$h_{\rm rad,D}$	$h_{\mathrm{D}}$
1.3	0.0001	344.45	2597.75	49.59	319.097
1.3	0.001	1290.83	1655.44	60.49	320.99
1.3	0.01	1380.58	1565.25	61.05	321.448

 $d_{\rm p}=1.030$  mm; Experience 9.

The CFD simulations carried out here have shown that some operating parameters and properties can be of crucial importance in simulations of the heat transfer process dealt with in this article. On the basis of the sensitivity analysis, it must be pointed out that a precise estimation of the values of parameters like  $f_{\rm B}$  and  $t_{\rm c}$ , as well as the absorption index, are essential for a good evaluation of heat transfer coefficients (independently of the modeling/simulation methodology).

#### **Conclusions**

The heat transfer between the dense phase of a high temperature bubbling fluidized bed and an immersed surface has been studied by means of CFD simulations. For this purpose, FLUENT 6.3.26 code and its mesh generator GAMBIT 2.4.6 code were used. Then, a valid and rigorous methodology for evaluating heat transfer rates between dense phase packet and an immersed surface has been established and tested.

The results from CFD simulations were compared and discussed with experimental data reported by Ozkaynak et al.21,22 and also with predicted values from the mechanistic model GHM.

A comparison with experimental data found in the literature was carried out to validate the use of empirical correlations adopted for time parameters. It has been shown that both,  $t_c$  and  $f_B$  along with the absorption index are the most important parameters to be evaluated to represent the wallto-bed heat transfer transient nature.

Different operating conditions were selected to carry out the study. High temperatures and different particle sizes adopted in simulations allow to cover different heat transfer regimes where the solid conductive and the gas convective contributions are dominant mechanisms altogether with the radiant heat transfer.

The temperature distribution inside the particles of the packet in contact with the immersed surface depends on both conduction and radiation. Consequently, it is essential to consider the interaction between the two mechanisms, as it is carry out in CFD calculations.

To identify the effect of some of the main parameters (void fraction in the dense phase, absorption, and scattering coefficients as well as the contact time and bubble fraction) on the heat transfer coefficients, several simulations were performed. These parameters were varied in a reasonable range for operating conditions revealing that  $t_c$  and  $f_B$  are the most important ones in the wall-to-bed heat transfer evaluation. Also, it is shown that at high operating temperatures,  $k_a$  plays an important role in the heat transfer process.

Possible particle motion near the wall can require some modifications in the simulation methodology, which can be considered as a future perspective of the work.

Small differences were found between CFD results for radiant and global heat transfer coefficients and most of the experimental results dealt with in the paper. The same conclusion can be established with respect to GHM's predictions which in turn provide a new strong evidence to validate the application of this mechanistic model. In this context, the results indicate that both the implementation of a microscopic simulation by CFD and the application of the GHM to quantify the heat transfer between the emulsion phase and a surface may result convenient, but it is necessary to have in mind that the application of GHM is very useful and simple. When comparing the GHM use with CFD simulations it is important to emphasize that the information concerning solid properties required by FLUENT is much more difficult to find than the relatively simpler requirements involved in layer properties evaluation for GHM. In this sense, CFD can be considered here as a "virtual experimental work" but the use of the GHM, involving only simple algebra and numerical calculations, can be emphatically recommended.

#### **Acknowledgments**

The authors acknowledge the financial support of the National University of Comahue and CONICET (Consejo Nacional de Investigaciones Científicas y Técnicas), Argentina. G. Mazza is a research member of CONICET. J. Soria is a Ph.D. student financially supported by the Argentine Agency of Scientific and Technological Promotion (ANP-

#### **Notation**

Ar = Archimedes number, dimensionless

Bi = Biot number, dimensionless

 $C_{\rm p}=$  particle specific heat capacity, kJ/kg/K

 $d_{\rm B} =$ bubble diameter, m

 $d_{\rm e} =$  equivalent diameter, m

 $D_{\rm L}=$  bed diameter, m

 $d_{\rm p} = {\rm particle\ diameter,\ mm}$ 

 $d_{\rm T}$  = probe diameter, m

 $f_{\rm B}=$  volumetric bubble fraction, dimensionless

 $F_{\rm Bw} = {\rm view \ factor, \ dimensionless}$ 

 $f_{\rm D}$  = time fraction for the dense phase, dimensionless

h = total heat transfer coefficient, W/m<sup>2</sup>/K

 $h_{\rm B} = \text{bubble-phase total heat transfer coefficient}, W/m^2/K$ 

 $h_{c,B}$  = bubble-phase convective heat transfer coefficient, W/m<sup>2</sup>/K  $h_{\rm D} =$  dense-phase total heat transfer coefficient, W/m<sup>2</sup>/K

 $h_{pg}$  = gas-particle heat transfer coefficient, W/m<sup>2</sup>/K

 $h_{\rm rad}$  = radiative heat transfer coefficient, W/m<sup>2</sup>/K

 $h_{\rm rad,B} = {\rm radiative\ heat\ transfer\ coefficient\ in\ the\ bubble-phase,\ W/m^2/K}$ 

 $h_{\rm rad,D}$  = radiative heat transfer coefficient in the dense-phase, W/m<sup>2</sup>/K

 $I = \text{radiation intensity, W/m}^2$ 

 $k_{\rm a}=$  absorption index, dimensionless

k = thermal conductivity, W/m/K

 $L_{\rm w} = {\rm vertical\ immersed\ surface\ length,\ m}$ 

m =complex refractive index, dimensionless

n = real component of the complex refractive index, dimensionless

 $q_{\rm D} = \text{total heat flux due to the dense phase, W/m}^2$ 

 $q_{\text{rad,D}}$  = radiant heat flux due to the dense phase, W/m<sup>2</sup>

 $\vec{r}$  = position vector

 $Re_{\rm D} = {\rm Reynolds}$  number for the dense phase, dimensionless

 $Re_{\rm mf} =$  Reynolds number at minimum fluidization condition, dimensionless

s = path length, m

 $\vec{s}$  = direction vector

 $\vec{s}' = \text{scattering direction vector}$ 

 $t_{\rm c} = {\rm contact\ time,\ s}$ 

 $T_{\rm F} = {\rm bulk} \; {\rm bed} \; {\rm temperature}, \; {\rm K}$ 

 $T_{\rm w}$  = immersed surface wall temperature, K

 $T_{\rm wCu} = {\rm surface}$  temperature of the cooper face, K

 $u_{\rm B}=$  bubble rising velocity, m/s

U= superficial gas fluidizing velocity, m/s

 $U_{\rm D} = \text{superficial gas velocity in the dense phase, m/s}$ 

 $U_{
m mf}=$  superficial gas velocity at minimum fluidization conditions, m/s

Z = effective length in Bock's correlation, m

#### Greek letters

 $\beta_{abs}$  = absorption coefficient, dimensionless

 $\beta_{\rm sca}=$  scattering coefficient, dimensionless

 $\delta = \text{porosity}, \text{dimensionless}$ 

 $\Omega'$  = solid angle

 $\varepsilon_{\rm p}=$  particle emissivity, dimensionless  $\lambda=$  wavelength,  $\mu{\rm m}$ 

 $\mu = \text{gas viscosity, kg/m/s}$ 

 $\rho_{\rm g} = {\rm gas \ density, \ kg/m^3}$ 

 $\rho_{\rm p}=$  particle density, kg/m<sup>3</sup>

 $\dot{\sigma} = \text{Stefan-Boltzmann constant}, 5.672 \cdot \times 10^{-8} \text{ W/m}^2/\text{K}^4$ 

 $\phi$  = phase function

 $\varphi = \text{distance from the distributor plate to probe position, m}$ 

#### Subscripts

B = bubble

D = dense phase

g = gas

p = particle

rad = radiant component

#### Literature Cited

- 1. Mickley HS, Fairbanks DF. Mechanism of heat transfer to fluidized beds. AIChE J. 1955;1:374-384.
- 2. Chen JC. Surface contact—its significance for multiphase heat transfer: diverse examples, 2001 Max Jacob Memorial Award Lecture. J Heat Transfer. 2003;125:549-566.
- 3. Ozkaynak TF, Chen JC. Average residence times of emulsion and void phases at the surfaces of heat transfer tubes in fluidized beds. AIChE Symp Ser. 1978;74:c1-c9.
- 4. Chen X, Louge M. Heat transfer enhancement in dense suspensions of agitated solids. Part II: experiments in the exchange limit, Int J Heat Mass Transfer. 2008;51:5119-5129.
- 5. Sidorenko I, Looi AY, Rhodes M. Particle motion near the wall of a fluidized bed at elevated pressure. Ind Eng Chem Res. 2004;43: 5562-5570.
- 6. Molerus O, Burshka A, Dietz S. Particle migration at solid surface and heat transfer in bubbling fluidized beds-1. Particle migration system. Chem Eng Sci. 1995;50:871-877.
- 7. Cody GD, Johri J, Goldfarb D. Dependence of particle fluctuation velocity on gas flow, and particle diameter in gas fluidized beds for monodispersed spheres in the Geldart B and A fluidization regimes. Powder Technol. 2008;182:146-170.
- 8. Chen X, Louge M. Heat transfer enhancement in dense suspensions of agitated solids. Part I: Theory Int J Heat Mass Transfer. 2008:51:5108-5118.
- 9. Yoshida K, Kunii D, Levenspiel O. Heat transfer mechanisms between wall surface and fluidized bed. Int J Heat Mass Transfer. 1969:12:529-536.
- 10. Zarghami R, Mostoufi N, Sotudeh-Gharebagh R. Particle-Wall Contact Time in Fluidized Beds. Proceedings of the third IASME/ WSEAS International Conference on Heat Transfer, Thermal Engineering and Environment, Corfu, Greece, 2005:85-90.
- 11. Wang L, Wu P, Ni X. Surface-particle-emulsion model of heat transfer between a fluidized bed and an immersed surface. Powder Technol. 2005;149:127-138.

- 12. Mazza GD. Análisis de la Transferencia de Calor Entre un Lecho Fluidizado y Superficies Sumergidas. PhD Thesis. Argentina: Chemical Engineering Department, Faculty of Engineering, University of La Plata, 1993.
- 13. Mazza GD, Mariani NJ, Barreto GF. Evaluation of overall heat transfer rates between bubbling fluidized beds and immersed surfaces. Chem Eng Commun. 1997;162:93-123.
- 14. Mazza GD, Bressa SP, Barreto GF. On the validity of the addition of independent contribution for evaluating heat transfer rates in gas fluidized beds. Powder Technol. 1997;90:1-11.
- 15. Gabor JD. Wall-to-bed heat transfer in fluidized and packed beds. Chem Eng Prog Symp Ser. 1970;66:76-86.
- 16. Mazza GD, Barreto GF. Analysis of models for heat transfer between gas-fluidized beds and immersed surfaces at high temperatures. Powder Technol. 1993;75:173-179.
- 17. Mazza GD, Barreto GF. The gas contribution to heat transfer between fluidized beds of large particles and immersed surfaces. Int J Heat Mass Transfer. 1988;31:603-614.
- 18. Chandran R, Chen JC. A heat transfer model for tubes immersed in gas fluidized beds. AIChE J. 1985;31:244-252.
- 19. Yoshida K, Ueno T, Kunii D. Mechanism of bed-wall heat transfer in a fluidized bed at high temperatures. Chem Eng Sci. 1974;29:77-82.
- 20. Mazza GD, Barreto, GF. Radiative heat transfer rates between gasfluidized beds and immersed surfaces. Trans Chem. 1994;72 (Part A):441-454
- 21. Ozkaynak TF, Chen JC, Frankenfield TR. Heat Transfer in High Temperature Fluidized Beds, TS-818. Bethlehem: Institute of Thermo-Fluid Engineering and Science, Lehigh University, 1981.
- 22. Ozkaynak TF, Chen JC, Frankenfield TR. An Experimental Investigation of Radiant Heat Transfer in High Temperature Fluidized Beds, Fluidization IV. Proceedings for the Fourth International Conference on Fluidization. Kashikokima, Japan, 1983.
- 23. Nijemeisland M, Dixon AG. Comparison of CFD simulations to experiment for convective heat transfer in gas-solid fixed bed. Chem Eng Sci. 2001;82:231-246.
- 24. Decker N, Glicksman LR. Heat transfer in large particle fluidized beds. Int J Heat Mass Transfer. 1983:26:1307–1320.
- 25. Baeyens J, Geldart D. Predictive calculations of flow parameters in gas fluidized beds and fluidization behavior of various powders. Proc Int Symp Fluid Appl. 1974;163-169.
- 26. Hilligardt K, Werther J. Local bubble hold-up and expansion of gassolid fluidized beds. Germ Chem Eng. 1986;9:215-221.
- 27. Bock HJ. Heat Transfer in Fluidized Beds. Preprints Fourth International Conference on Fluidization. Kashikojima, Japan, 1983;5.2.1–5.2.8.
- 28. Ozkaynak TF, Chen JC. Emulsion phase residence time and its use in heat transfer models in fluidized beds. AIChE J. 1980;26:544-550
- 29. Hamidipour M, Mostoufi N, Sotudeh-Gharebagh R, Chaouki J. Experimental investigation of particle contact time at the wall of gas fluidized beds. Chem Eng Sci. 2005;60:4349-4357.
- 30. Hua Y, Flamant G, Lu J, Gauthier D. 3D modeling of radiative heat transfer in circulating fluidized bed combustors: influence of particle composition. Int J Heat Mass Transfer. 2004:48:1145–1154.
- 31. Lacroix D, Parent G, Asllanaj F, Jeandel G. Coupled radiative and conductive heat transfer in a non-grey absorbing and emitting semitransparent media under collimated radiation. J Quant Spectroscopy Radiat Transfer. 2002;75:589-609.
- 32. Yamada J, Kurosaki Y, Satoh I, Shimada K. Radiative heat exchange between a fluidized bed and heated surface. Exp Therm Fluid Sci. 1995;11:135-142.
- 33. Liley PE. Physical properties, Vol. 5. In: Schlünder EU, editor. Heat Exchanger Design Handbook. Hemisphere Publishing Corporation, 1983.

Manuscript received Apr. 21, 2010, revision received Oct. 26, 2010, and final revision received Jan. 24, 2011.